



## *In-situ* magnetic activated carbon produced from sludge, straw and steel slag for the effective adsorption of methylene blue

Cong Liang<sup>a,b</sup>, Qingguo Tang<sup>a,b,\*</sup>, Weiwei Zhao<sup>a,b</sup>, Yuanhang Han<sup>a,b</sup>, Yinlong Qiao<sup>a,b</sup>, Xinhui Duan<sup>a,b,\*</sup>, Jinsheng Liang<sup>a,b</sup>

<sup>a</sup>Institute of Power Source and Ecomaterials Science, Hebei University of Technology, Tianjin, CN 300401, emails: tangqingguo@hebut.edu.cn (Q.G. Tang), dxh1191984@aliyun.com (X.H. Duan)

<sup>b</sup>Key Laboratory of Special Function Materials for Ecological Environment and Information, Hebei University of Technology, Tianjin, CN 300401, emails: liang1097@126.com (C. Liang), 2628361116@qq.com (W.W. Zhao), 2201245939@qq.com (Y.H. Han), 1041621982@qq.com (Y.L. Qiao), liangjinsheng@hebut.edu.cn (J.S. Liang)

Received 11 January 2023; Accepted 12 May 2023

### ABSTRACT

In order to achieve the goal of green and sustainable development, solid waste of sludge, straw and steel slag were used as raw materials for the preparation of *in-situ* magnetic activated carbon (MAC) by chemical activation and co-pyrolysis, and was then used to remove methylene blue (MB). The MAC with the highest specific surface area (359 m<sup>2</sup>/g) was obtained at 750°C, and the *in-situ* magnetization was achieved by reducing the iron oxides in steel slag to Fe<sub>3</sub>O<sub>4</sub> and Fe<sup>0</sup>, resulting in a saturated magnetization of 8.69 emu/g, this allowed for easy separation using a magnet. Batch adsorption of MB onto MAC was studied, indicating the removal efficiency of methylene blue was higher than 95% under room temperature at pH = 8 while the dosage of MAC was 1 g/L. Adsorption kinetic and isotherm studies indicated the adsorption of methylene blue onto MAC involved multilayer physisorption with intraparticle diffusion and chemisorption as the rate-limiting steps. The maximum calculated adsorption capacity of MB was 283 mg/g; thermodynamic analysis showed the adsorption was spontaneous and endothermic. The adsorption mechanism of methylene blue onto MAC involved electrostatic attraction, formation of hydrogen bonds and the interaction of  $\pi$  electron system.

**Keywords:** Solid waste; Activated carbon; *In-situ* magnetization; Methylene blue; Adsorption mechanism

### 1. Introduction

Currently, over 100,000 types of dyes are utilized annually in the textile industry, and it is reported that about 20% of the applied dyes are discharged into water, which will bring serious damage to the ecological environment [1]. Methylene blue (MB), a widely used organic dye, is difficult to be biodegraded or photodegraded in water due to its deep color and stable structure, and it is reported to be carcinogenic to humans [2]. Various methods have been developed for the treatment of MB, involving adsorption,

photodegradation, chemical oxidation coagulation–flocculation, electrochemical treatment and so on [3]. Among these methods, adsorption stands out for its high efficiency, low cost, and ease of operation. The commonly used adsorbents are activated carbon, porous ceramics, aerogels, mesoporous silica and other porous materials [4]. In terms of cost-effectiveness, activated carbon prepared from waste materials has been the potential choice of adsorbents.

As the significant municipal solid waste of sewage treatment plants, sludge contains a variety of microorganisms, undigested organic matters (such as paper, plant residues, oil, manure) [5], and usually landfilled and

\* Corresponding authors.

incinerated, yet these traditional treatments could also cause the secondary pollution [6]. Due to the consideration of sustainable development, thermal processing of the sludge has come into view [7,8], and as a pyrolysis product, sludge-based activated carbon (SAC) with good porosity can be used to treat wastewater as a reuse method [9–11]. However, compared with the mainstream adsorbents, the limited carbon content of sludge led to the low specific surface area and poor adsorption properties [12]. In order to enhance the performance of the pure SAC, researchers have experimented with mixing sludge with agricultural waste such as straw and fruit shells. These composite adsorbents had demonstrated higher adsorption capacities, for example, Yang et al. [13] prepared composite activated carbon by mixing sludge with coconut shell and using chemical activation and two-step pyrolysis, the prepared adsorbent provided an adsorption capacity of 602 mg/g for methylene blue; Kang et al. [14] reported the preparation of activated carbon with 88.19% removal of amoxicillin by compounding sludge with walnut shell.

In general, carbon adsorbents are usually powders or fine particles, which are difficult to be separated and recycled effectively from wastewater, thus it is a common solution to prepare magnetic adsorbents for recycling after saturation. Magnetic adsorbents are commonly prepared by chemical co-precipitation of divalent or trivalent iron salts, which have a great demand for pure chemicals [15–17]. In order to reduce development costs, researchers are constantly seeking alternative raw materials and simpler methods. One such method of obtaining  $\text{Fe}^0$  or  $\text{Fe}_3\text{O}_4$  from industrial solid wastes with high iron content through reduction is starting to come into view. For example, Wang et al. [18] mixed black liquor with red mud and prepared zero-valent iron-embedded biochar during pyrolysis, where the oligomers in black liquor acted as reductants for red mud; Kazak [19] used sucrose and red mud as raw material and obtained magnetic adsorbents with saturation magnetization of 15.4 and 17 emu/g, at 750°C and 1,000°C through co-pyrolysis, which could be easily separated using a magnet. Steel slag is a solid waste discarded from the steelmaking process; and it was reported that only about 20% of waste steel slag was properly disposed in China [20]. Steel slag contains a large number of metal oxides, with total FeO and  $\text{Fe}_2\text{O}_3$  usually exceeding up to 38% [21]. In contrast, the reduction of iron oxides in steel slag and its application to the field of magnetic adsorbents has been rarely found: Thuan et al. [22] prepared cross-linked magnetic chitosan particles from steel slag and shrimp shells; Basaleh et al. [23] used the AA (acrylamide acrylic) to modify the steel slag, for the preparation of a magnetic polymeric composite to remove dyes.

In this context, this study is the first to prepare an *in-situ* magnetic activated carbon (MAC) by using sludge, straw as the primary carbon source and steel slag as the primary magnetic source through chemical activation and co-pyrolysis. The *in-situ* magnetization effectively reduces the use of pure chemicals, and the prepared adsorbent was subjected to MB's removal to evaluate the adsorption performance. It was hoped to provide a new idea for the disposal of multiple solid wastes towards high-quality utilization and to achieve the goal of treating wastewater with waste.

## 2. Materials and methods

### 2.1. Materials

Sludge was obtained from a sewage treatment plant in Tanggu, Tianjin; the wheat straw was collected from the outskirts of Tianjin; and the steel slag was provided by Tianjin Xintiengang Steel Group. The main composition analysis of sludge and steel slag mentioned above are shown in Table 1. The chemical reagents used in the experiments included KOH (analytical grade), HCl (analytical grade), methylene blue (MB), were all purchased from Kmart (Tianjin) Chemical Technology Co.

### 2.2. Preparation of the MAC

After drying and grinding into fine particles (through 60 mesh sieve), the sludge, straw and steel slag were mixed at a weight ratio of 2:2:1 and then impregnated in 3 M KOH with the ratio of 1:4 for 12 h. The mixtures were oven-dried for impregnation. After that, impregnated samples were carbonized under a nitrogen atmosphere using a tube-type resistance furnace at 650°C, 700°C, 750°C and 800°C for 2 h, and the heating rate was kept at 10°C/min. Carbonized samples were washed with deionized water to neutral, dried at 105°C to obtain a series of adsorbents. The resultant samples were labelled as MAC-650, MAC-700, MAC-750 and MAC-800.

### 2.3. Characterization

The thermal stability of the raw materials was analyzed using the thermogravimetric analyzer (Rigaku TG-DTA8122, Japan) under the nitrogen atmosphere. The microscopic morphology of raw materials and MACs were observed by field emission environmental scanning electron microscopy (Quanta 450 FEG, FEI Co., Hong Kong). The specific surface area and pore size distribution were measured by the isotherms of  $\text{N}_2$  adsorption by automatic chemical physical adsorption instrument (Autosorb iQ, Quantachrome Co., USA). The surface functional groups of the materials were observed by FTIR spectrophotometer (V80, Bruker German). The saturation magnetization intensity of MAC was determined using the vibrating sample intensity magnetometer (7407, Lakeshore, USA). The crystallographic property of the

Table 1  
Main composition analysis of the sludge and steel slag

	Sludge	Steel slag
$\text{SiO}_2$ (%)	18.7	5.39
$\text{Al}_2\text{O}_3$ (%)	16.2	0.99
CaO (%)	8.22	33.0
$\text{P}_2\text{O}_5$ (%)	4.55	1.06
$\text{TFe}_2\text{O}_3$ (%)	15.5	46.0
MnO (%)	1.38	6.64
C (%)	29.8	–

$\text{TFe}_2\text{O}_3$  means the total content of all iron elements in geological and mineral-like materials, which can also be expressed as TFe (total iron).

materials was recorded by X-ray diffractometer (SmartLab 9kW, RIKEN, Japan Co.). The surface composition of the adsorbent was analyzed by X-ray photoelectron spectroscopy (Thermo Scientific K-Alpha, USA). And the zero potential point of the adsorbent was determined by zeta potential analyzer (Malvern Zetasizer Nano ZS ZEN3600, UK).

#### 2.4. Batch adsorption experiments

A stock solution of 1,000 mg/L MB was prepared and this stock solution diluted all the initial concentrations of methylene blue used in experiments. And the adsorption was performed in a 100 mL conical flask in a constant temperature air bath shaker at 150 rpm, 0.1 M of HCl and KOH were used to adjust the pH of methylene blue solution.

200 mg/L of methylene blue was used to determine the effects of contact time (30~1,440 min), the dosages of adsorbent (0.2~1.2 g/L), and the pH value of MB (2~12). Besides, several kinds of salts solutions were used (NaCl, CaCl<sub>2</sub>, NaHCO<sub>3</sub> and Na<sub>2</sub>CO<sub>3</sub>) to investigate the effect of common salts on the adsorption performance of methylene blue.

The concentration of the adsorbed solution was determined using a UV-Vis spectrophotometer at  $\lambda = 665$  nm, the amount of methylene blue adsorbed and removal efficiency were calculated by the following equations:

$$q_e = \frac{(C_0 - C_e) \times V}{w} \quad (1)$$

$$\eta = \frac{C_0 - C_e}{C_0} \times 100\% \quad (2)$$

where  $q_e$  (mg/g) is the adsorption capacity at equilibrium;  $\eta$  (%) is the removal efficiency;  $C_0$  (mg/L) and  $C_e$  (mg/L) are the initial and equilibrium concentrations of methylene blue;  $V$  (L) is the volume of methylene blue solution;  $w$  (g) is the mass of MAC.

From the best conditions defined, the studies of adsorption kinetic were performed using initial MB concentrations of 200, 300 and 400 mg/L at 298 K in 30, 60, 120, 240, 480, 720 and 1,440 min. The pseudo-first-order model, pseudo-second-order model, Elovich model and Webber–Morris model were used to analysis the adsorption kinetics. The models mentioned above were determined by the Eqs. (3)~(6):

$$q_t = q_e (1 - e^{-K_1 t}) \quad (3)$$

$$q_t = \frac{q_e^2 K_2 t}{1 + q_e K_2 t} \quad (4)$$

$$q_t = \frac{1}{b} \ln(1 + a \times b \times t) \quad (5)$$

$$q_t = K_{id} t^{1/2} + C \quad (6)$$

where  $q_t$  (mg/g) is the adsorption capacity at time  $t$  (min),  $K_1$  (1/min),  $K_2$  (g/mg·min) and  $a$  (mg/g·min) are the adsorption rate constant corresponding to the first-order, second-order kinetic models and Elovich model,  $b$  (g/mg) is the parameter related to the degree of adsorbent surface coverage and

chemisorption activation energy,  $K_{id}$  is the internal diffusion rate constant and  $C$  is the constant involving thickness and boundary layer.

The adsorption isotherms and thermodynamics were studied by varying the initial concentrations of MB at 298, 308 and 318 K. The isotherms were fitted using the Langmuir, Freundlich, Temkin and Sips models. The models above were determined by Eqs. (7)–(10):

$$q_e = \frac{q_m K_L C_e}{1 + K_L C_e} \quad (7)$$

$$q_e = K_F C_e^{1/n} \quad (8)$$

$$q_e = \frac{RT}{\beta} \ln(\alpha \cdot C_e) \quad (9)$$

$$q_e = \frac{K_s C_e^{b_s}}{1 + a_s C_e^{b_s}} \quad (10)$$

where  $q_m$  (mg/g) represents the maximum adsorption capacity, and  $K_L$  (L/mg),  $K_F$  (mg/g),  $\alpha$  (L/g),  $K_s$  (L/g) and  $a_s$  (L/mg) are the constants related to the adsorption model mentioned above,  $n$  is dimensionless parameter,  $\beta$  (J/mol) is the Temkin's constant associated with the heat of adsorption, and  $b_s$  is the Sips model exponent.

The thermodynamic parameters of the adsorption process were calculated by the following equations:

$$\Delta G = -RT \ln K_c \quad (11)$$

$$K_c = \frac{q_e}{C_e} \quad (12)$$

where  $\Delta G$  (kJ/mol) is the Gibb's free energy change;  $R$  (8.314J/mol·K) is the molar gas constant;  $T$  (K) is the thermodynamic temperature;  $K_c$  is the thermodynamic equilibrium constant.

And the change in enthalpy ( $\Delta H$ , kJ/mol) and the change in entropy ( $\Delta S$ , J/mol) were determined by the Van't Hoff equation:

$$\ln K_c = -\frac{\Delta H}{RT} + \frac{\Delta S}{R} \quad (13)$$

### 3. Results and discussion

#### 3.1. Characterization of raw materials and MACs

The pyrolysis temperature is an important factor affecting the performance of biochar. The TG and DTG curves of sludge, steel slag and straw were tested from room temperature to 800°C under nitrogen conditions to determine the thermal stability of the raw materials, and the results are shown in Fig. 1.

According to Fig. 1, The TG curve of steel slag was relatively flat, and the mass no longer changed after 680°C, the total weight loss was about 10%. There were two obvious weight loss peaks between 105°C and 656°C in terms of the corresponding DTG curve, the former should be the evaporation of water, and the latter was the decomposition of

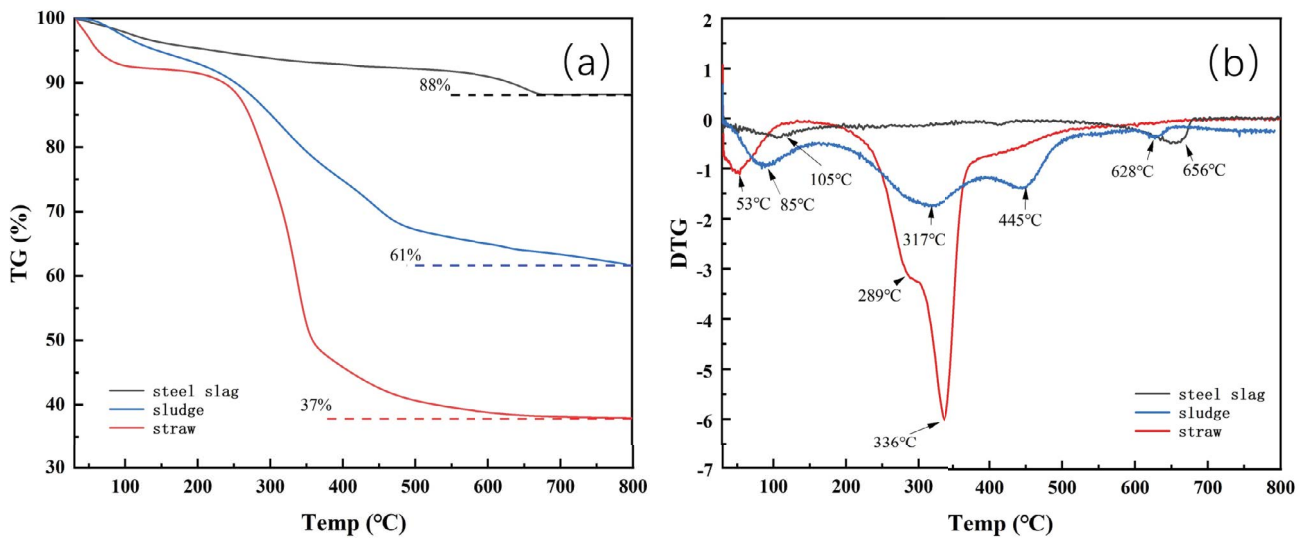


Fig. 1. (a) Thermogravimetric curves and (b) DTG curves of raw materials.

inorganic minerals in steel slag. The total weight loss of the sludge was about 40% according to the TG curve due to the decomposition of water and inorganic minerals, the sludge had two weight loss peaks at 317°C and 445°C, corresponding to the decomposition of organic matters in the sludge with a mass loss of 25%. The weight loss of straw during pyrolysis was concentrated below 100°C and 250°C–400°C due to the decomposition of water and lignin, cellulose, hemicellulose etc., with a total mass loss of more than 60%. Based on these results, it was feasible to set the pyrolysis temperature at 650°C–800°C.

Table 2 shows the Brunauer–Emmett–Teller (BET) data and yield of MACs. As can be seen from the Table 2, the specific surface areas of MACs were all higher than 200 m<sup>2</sup>/g, with MAC-750 being the highest at 359 m<sup>2</sup>/g, indicating that 750°C was an ideal pyrolysis condition. The surface area of MAC-800 decreased, which could be attributed to the hole collapse caused by higher temperatures [13]. So, MAC-750 would be the best sample for subsequent adsorption and characterization.

The N<sub>2</sub> adsorption isotherm and pore size distribution plot of MAC-750 are shown in Fig. 2a and b. As reported by IUPAC, the N<sub>2</sub> adsorption isotherm of MAC-750 can be classified as type IV because of its Obvious inflection point at a low  $P/P_0$  region and its hysteresis, which suggested the mesoporous properties of the adsorbent [24].

The surface morphology of sludge, steel slag and MAC-750 were observed by scanning electron microscopy (Fig. 2c–f). As shown in the images, the surface of MAC-750 presents a rough, porous structure, this was caused by the chemical activation and co-pyrolysis; in addition, the catalytic of the iron-based components of raw materials also plays an important role in the process of pore formation [19]. The formation of these pores gave the adsorbent a high specific surface area and provided many active sites.

Abundant functional groups of raw materials and MAC-750 were observed by Fourier-transform infrared spectroscopy (FTIR), and the spectra are presented in Fig. 3a. Most of the functional groups of raw materials were found

Table 2  
Brunauer–Emmett–Teller data and yield of magnetic activated carbons

	Surface area (m <sup>2</sup> /g)	Average pore diameter (nm)	Total pore volume (cm <sup>3</sup> /g)	Yield (%)
MAC-650	212	6.40	0.340	70.2
MAC-700	297	5.14	0.382	67.5
MAC-750	359	4.11	0.370	64.8
MAC-800	303	4.62	0.335	59.4

in MAC-750, among which the characteristic peaks at 3,394 and 1,635 cm<sup>-1</sup> were attributed to the vibration of O–H [25,26], the peaks at 2,929 and 2,848 cm<sup>-1</sup> were due to the asymmetric stretching and symmetric stretching vibration of C–H [27,28]. The decrease of these peaks in MAC-750 was caused by dehydration and demethylation reaction during the pyrolysis. Besides, the peaks at 1,418 cm<sup>-1</sup> indicated the vibration of C=C in the aromatic compounds, and the peak at 1,003 cm<sup>-1</sup> was ascribed to the stretching of C–O–C [29]. It has been reported that the characteristic peaks at 694 cm<sup>-1</sup> can be attributed to the vibration of C–H in aromatics [30]. By the way, the peak at 578 cm<sup>-1</sup> was considered Fe–O [19], which could be observed in steel slag, either.

Magnetic measurement of MAC-750 was investigated through vibrating sample magnetometer at room temperature, and the magnetization curve is presented in Fig. 3b. As shown in the curve, MAC-750 showed ferromagnetic properties supplied by the iron of the raw materials, and its saturation magnetization value calculated was 8.69 emu/g, which could be easily separated by a magnet according to the image in Fig. 3b.

The X-ray diffraction patterns of sludge, steel slag and MACs are presented in Fig. 4. As can be seen from the patterns, the original sludge and steel slag had complex compositions with lots of amorphous substances. After activation and pyrolysis, broad peaks appeared at the

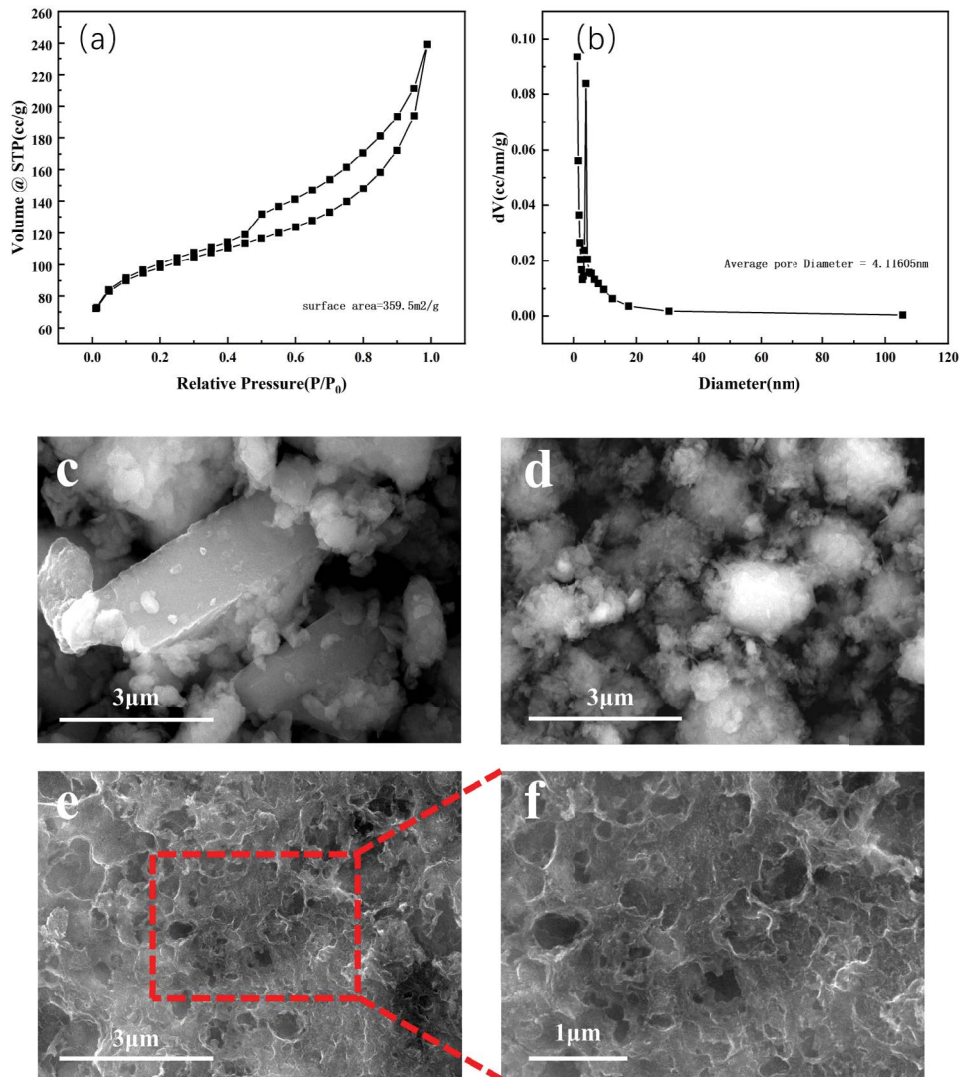


Fig. 2. (a) The  $N_2$  adsorption isotherm of MAC-750, (b) pore-size distribution of MAC-750, (c) 50,000 $\times$  magnification images of sludge, (d) steel slag, (e) MAC-750 and (f) 100,000 $\times$  magnification image of MAC-750.

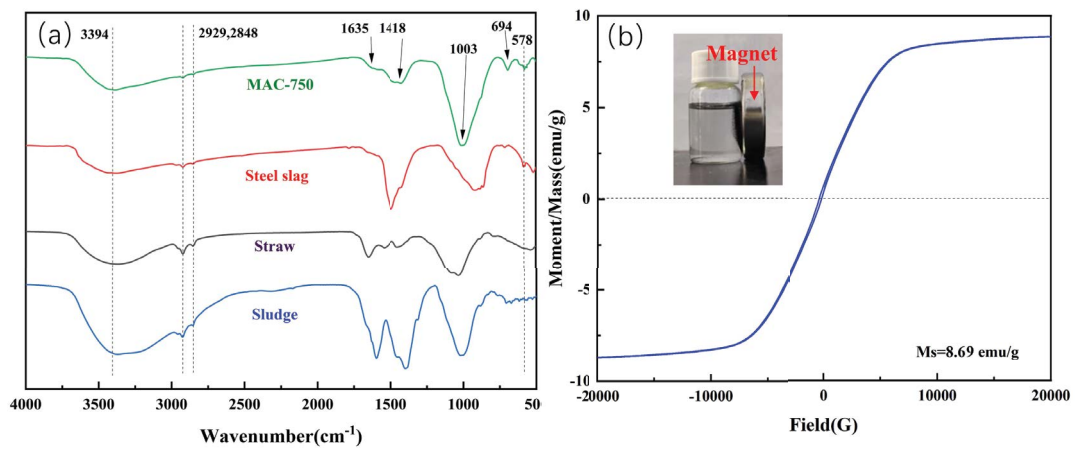


Fig. 3. (a) Fourier-transform infrared spectra of MAC-750, steel slag, straw and sludge and (b) magnetization curve and separation image of MAC-750.

diffraction angles of  $20^{\circ}$ – $30^{\circ}$  (Fig. 4b), indicating the formation of additional amorphous substances. Besides, partially crystallized silicate minerals and  $\text{CaCO}_3$  in MACs decomposed with increasing temperature (Fig. 4b),  $\text{FeO}$  (JCPDS 46-1312) and  $\text{Fe}_2\text{O}_3$  (JCPDS 39-0238) in steel slag were reduced to  $\text{Fe}^0$  (JCPDS 99-0064) and  $\text{Fe}_3\text{O}_4$  (JCPDS 79-0416) in the reductive atmosphere generated by the combustion of organic matter in the raw materials.

To further investigate the surface elements and the source of magnetism of the adsorbent, X-ray photoelectron spectroscopy was used, and the results are shown in Fig. 5. The atomic percentage of elements on the surface of MAC-750 was determined as: C (31.71%), O (53.56%), Si (8.64%), Al (3.89%), Fe (1.36%), Ca (0.84%). In the O1s spectrum, a distinct Fe–O peak (529.68 eV) was observed (Fig. 6d). In the Fe2p spectrum (Fig. 5e), two peaks at the binding energies

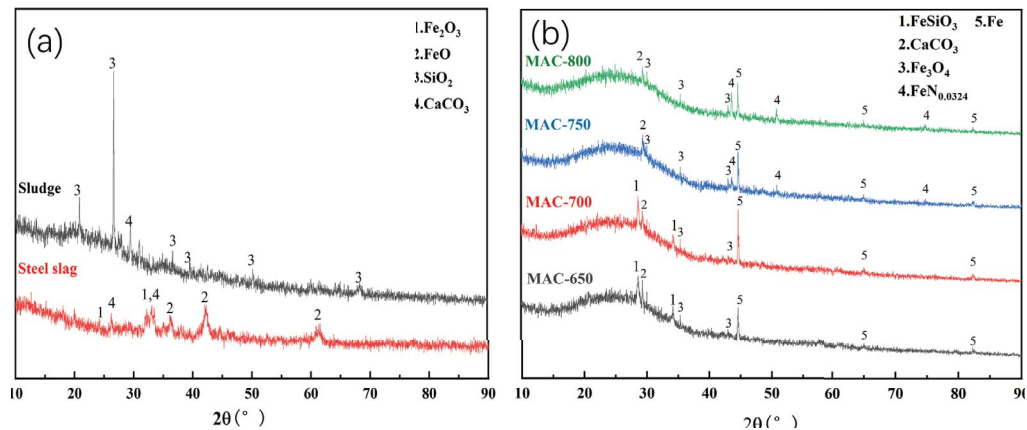


Fig. 4. X-ray diffraction patterns of (a) sludge, steel slag and (b) magnetic activated carbons.

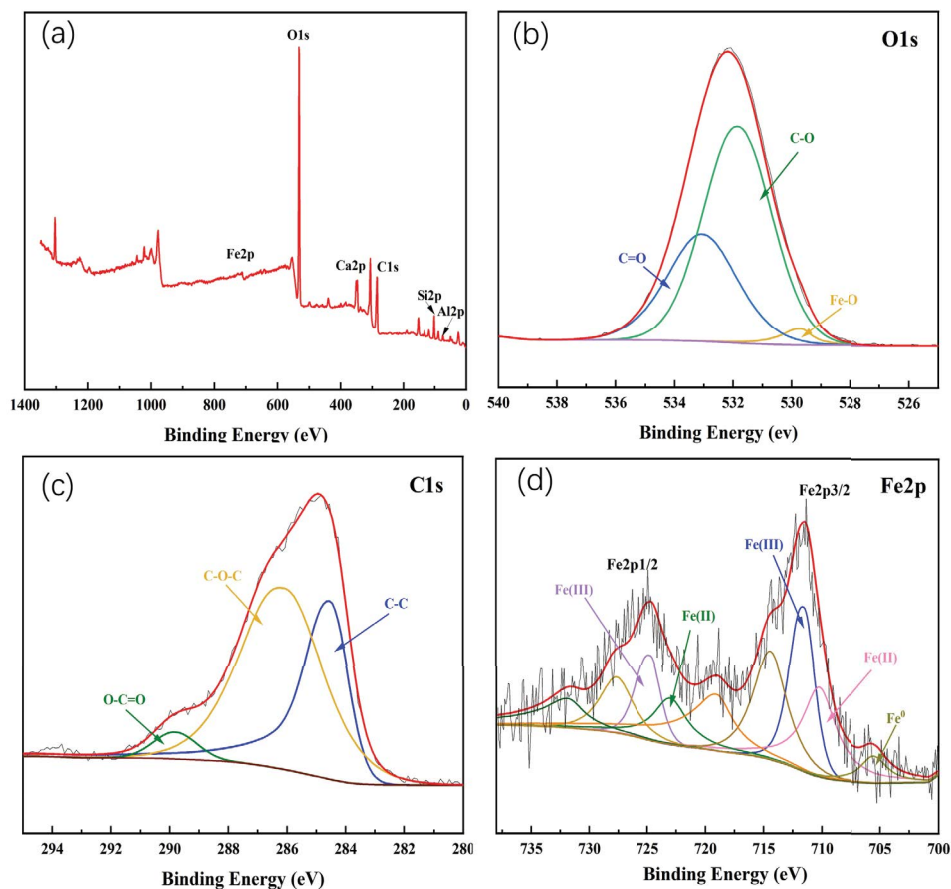


Fig. 5. X-ray photoelectron spectra of (a) MAC-750, (b) O1s, (c) C1s, and (d) Fe2p.

of 711.58 and 724.68 eV could be assigned to Fe(II) (710.18 and 722.98 eV) and Fe(III) (711.68 and 724.88 eV), respectively, which were considered as the characteristic peaks of  $\text{Fe}_3\text{O}_4$  [31]. Furthermore, the small peak at 705.78 eV corresponded to the reduced  $\text{Fe}^0$  [32].

### 3.2. Effects of the contact time, adsorbent dosages and initial pH

The effect of contact time on MB removal efficiency is shown in Fig. 6a (conditions: dosage of MAC = 1 g/L, total reaction volume = 50 mL, initial MB concentration = 200 mg/L at room temperature, and the pH was neutral). As shown from the image, the rate of adsorption of methylene blue onto MAC-750 was pretty fast at the beginning, the removal efficiency was higher than 70% in the first 30 min; and the adsorption almost reached equilibrium after 720 min, the removal efficiency reached 94.1%. This was attributed to the higher number of activated sites available on the MAC at the beginning; as the extension of the contact time, the limited number of activated sites controlled the efficiency of adsorption [33]. Accordingly, 720 min was selected as a fixed contact time in further experiments.

The effect of different adsorbent dosages on the methylene blue removal efficiency is shown in Fig. 6b (conditions: contact time = 720 min, total reaction volume = 50 mL, initial MB concentration = 200 mg/L at room temperature, and

the pH was neutral). It can be seen from the curve that the removal efficiency of methylene blue was positively correlated with the amount of adsorbent added. The removal efficiency of methylene blue increased significantly from 62% to 94% when the dosage was less than 1 g/L. However, the increase in the removal efficiency started to slow down when the dosage was higher than 1 g/L, which indicated that the additional adsorbents added did not promote the adsorption process due to the overlap of active sites [34]. Considering the removal efficiency, 1 g/L of adsorbent was chosen in the subsequent experiments.

Fig. 6c shows the MB removal efficiency of MAC-750 at different pH values (conditions: dosage of MAC = 1 g/L, total reaction volume = 50 mL, initial MB concentration = 200 mg/L at room temperature, contact time = 720 min). According to the curve, the removal efficiency increased with the increasing pH value. As the pH increased from 2 to 8, the adsorption efficiency was higher than 95%, this phenomenon could be due to the cationic nature of methylene blue and electrostatic effects [35]. The zero potential point ( $\text{pH}_{\text{zpc}}$ ) of MAC-750 was around 6.56, this led to the electrostatic repulsion between methylene blue and MAC when the  $\text{pH} < \text{pH}_{\text{zpc}}$ ; as the pH increased, the concentration of  $\text{H}^+$  in the solution decreased, and methylene blue would be more easily adsorbed on the adsorbent surface [36]. For economical and efficiency considerations, the pH was set to 8 in subsequent experiments.

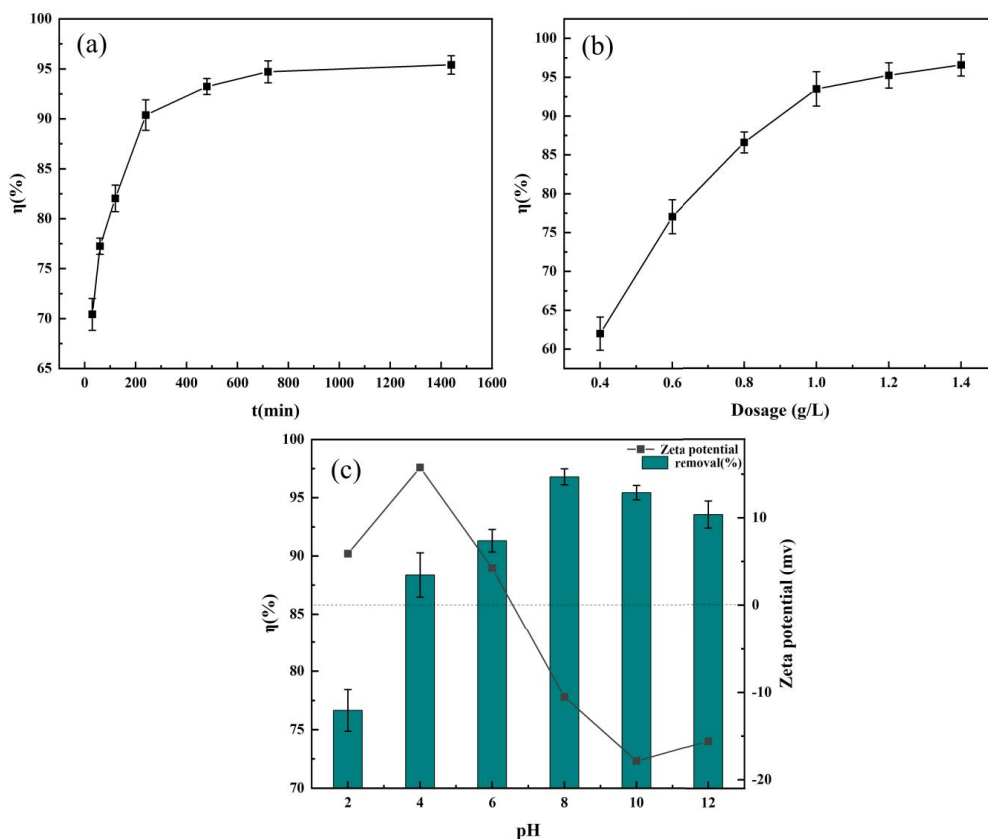


Fig. 6. (a) Effect of different contact time on the removal of methylene blue at room temperature, (b) effect of different adsorbent dosages on the removal of methylene blue at room temperature, and (c) effect of different initial pH on the removal of methylene blue at room temperature and zeta potential of MAC-750 ( $\text{pH}_{\text{zpc}} = 6.56$ ).

### 3.3. Effects of common salts on adsorption

Salts have been used in the dye application process, and it has been found that their presence may affect the adsorption of organic dyes by activated carbon. To examine the effect of common salts on adsorption capacity, 0.1 mol/L of NaCl, CaCl<sub>2</sub>, NaHCO<sub>3</sub> and Na<sub>2</sub>CO<sub>3</sub> were added to MB solutions and the results are shown in Table 3.

As shown in Table 3, the presence of NaCl and CaCl<sub>2</sub> in aqueous solutions had a negative effect on the adsorption of MB, and the effect of CaCl<sub>2</sub> was more significant. There are two possible reasons for this phenomenon. First, due to the electrostatic interaction between MAC

surface and methylene blue, the presence of NaCl and CaCl<sub>2</sub> enhanced the ionic strength in solution, leading to competitive adsorption with methylene blue [37]. Secondly, as these salts were added, the activity coefficient decreased, resulting in lower activity of dyes and active binding sites. However, the presence of Na<sub>2</sub>CO<sub>3</sub> and NaHCO<sub>3</sub> slightly enhanced the adsorption of methylene blue, which is consistent with the findings of Matias [26]. This is due to the hydrolysis of the added CO<sub>3</sub><sup>2-</sup> and HCO<sub>3</sub><sup>-</sup>, which created a weakly basic solution and increased the electrostatic attraction between the MAC and the dye solution, thus facilitating the adsorption [38].

Table 3  
Effect of common salts on methylene blue adsorption

System	Adsorption capacity for 300 mg/L methylene blue (mg/g)	Adsorption capacity for 500 mg/L methylene blue (mg/g)
H <sub>2</sub> O	239	278
NaCl	231	265
CaCl <sub>2</sub>	168	232
NaHCO <sub>3</sub>	246	289
Na <sub>2</sub> CO <sub>3</sub>	253	310

### 3.4. Studies of adsorption kinetics

Fig. 7a–c shows the fitting results of the pseudo-first-order, pseudo-second-order, Elovich and Webber–Morris models of the adsorption of different concentrations of methylene blue onto MAC-750, and the fitting parameters are shown in Table 4.

As can be seen from the curves, the amount of MB adsorbed increases rapidly during the early stages of adsorption and gradually approaches saturation as the contact time is extended. According to the fitting results, with the comparison of the pseudo-first-order model ( $R^2 = 0.622\text{--}0.713$ ), pseudo-second-order ( $R^2 = 0.912\text{--}0.954$ ) and Elovich ( $R^2 = 0.963\text{--}0.980$ ) showed better fitting performance for

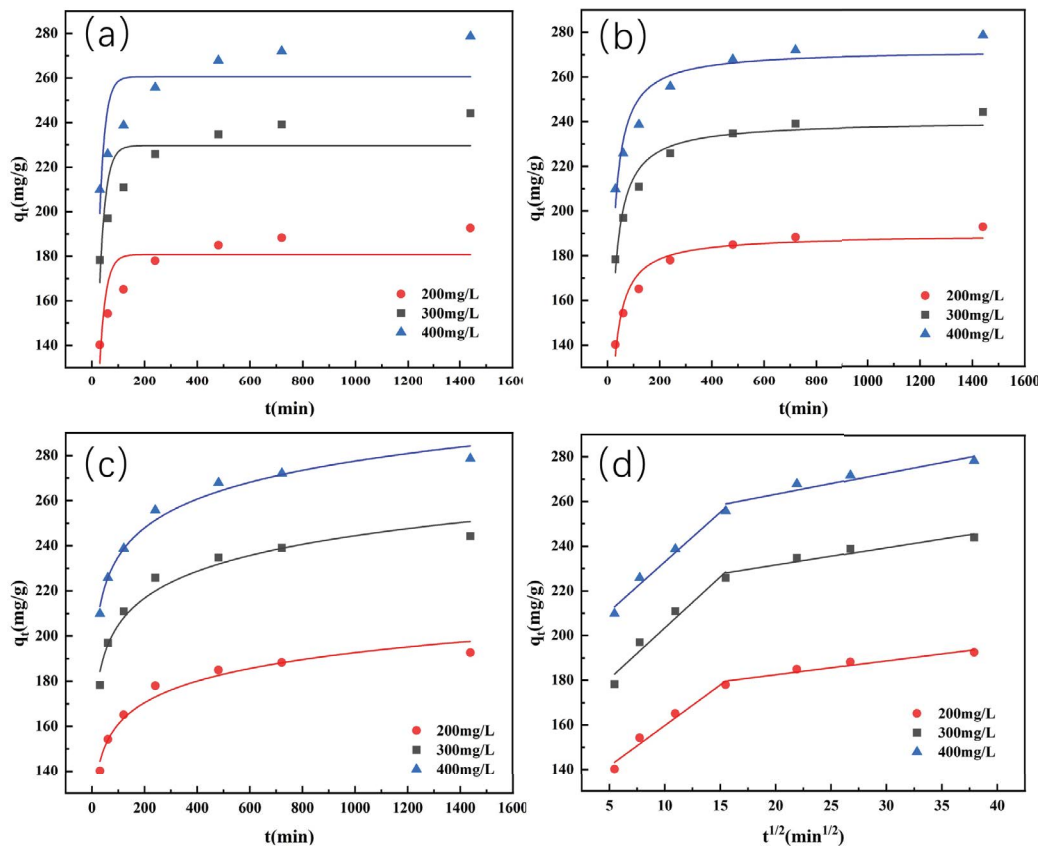


Fig. 7. Fitting results of (a) pseudo-first-order, (b) pseudo-second-order, (c) Elovich and (d) Webber–Morris model of methylene blue adsorption onto MAC-750.

Table 4  
Fitting parameters of the adsorption kinetic models of methylene blue adsorption onto MAC-750

Models	Parameters	200 mg/L	300 mg/L	400 mg/L
Pseudo-first-order	$q_e$ (mg/g)	181	230	261
	$K_1$ (1/min)	0.0434	0.0431	0.0484
	$R^2$	0.697	0.713	0.622
Pseudo-second-order	$q_e$ (mg/g)	189	240	272
	$K_2$ (g/mg-min)	0.000431	0.000354	0.00340
	$R^2$	0.946	0.954	0.912
Elovich	$a$ (mg/g-min)	88.4	89.1	199
	$b$ (g/mg)	13.8	17.2	18.4
	$R^2$	0.966	0.963	0.980
	$K_a$	3.63	4.56	4.44
	$C_a$	153	158	189
Webber–Morris	$R_1^2$	0.969	0.957	0.980
	$K_b$	0.629	0.788	0.965
	$C_b$	200	216	244
	$R_2^2$	0.929	0.920	0.905

the data. Theoretically, the pseudo-second-order model assumes the adsorption progress reflects the liquid film diffusion, surface adsorption and intraparticle diffusion, while the rate-limiting step is chemisorption [39], which provides a more comprehensive and accurate reflection of the adsorption progress than pseudo-first-order did. Moreover, Elovich model suggests the assumption that the adsorption sites of the adsorbent are inhomogeneous and display a variety of activation energy during the adsorption process [40]. So, the fitting results indicated that the adsorption of MB onto MAC-750 was a non-uniform diffusion process on the inhomogeneous surface rather than a simple primary reaction [36].

To further investigate the controlling factors of diffusion during adsorption, the Webber–Morris model was applied and the fitting results are shown in Fig. 7d and Table 4. As can be seen from the figure, the curve presented two linear segments, indicating that more than one rate-limiting step in control. Additionally, the intercepts of the linear segments were in an extensive range, demonstrating the significant influence of liquid film diffusion [41]. Therefore, the diffusion behavior of MB adsorption onto MAC-750 can be summarized as the following: firstly, methylene blue molecules rapidly diffused from the liquid phase to the outer surface of the adsorbent via liquid film diffusion, and then by intraparticle diffusion, MB molecules entered the internal pores and adsorbed onto active sites within the adsorbent until equilibrium was reached [42].

### 3.5. Studies of adsorption isotherm

Fig. 8a–d show the adsorption isotherms of MAC-750 at different ambient temperatures, and the fitting parameters are shown in Table 5.

As seen from the curves, the ambient temperature had a beneficial effect on the adsorption. The gradual increase in adsorption may be attributed to the fact that the MB comes into contact with the active sites of the adsorbent

more frequently as the temperature rises from 298 to 318 K [43]. The specific adsorption thermodynamics studies were elaborated on in the next section.

Besides, the adsorption of MB increased gradually with the increase in initial concentration. At lower concentrations of methylene blue, the adsorption increased rapidly. However, as the initial concentration of the dye continued to increase, the increase in adsorption began to converge towards a limit. The data were further analyzed using four isotherm models. The Langmuir model assumes that the adsorbent surface is homogeneous, with uniform adsorption energy at all adsorption sites, and that the adsorption process involves the formation of a unimolecular layer, and the theoretical maximum adsorption capacity is reached when the adsorbent surface is fully covered [44]. The Freundlich model describes multilayer adsorption on inhomogeneous surfaces, with the parameter  $1/n$  indicating the adsorption strength or surface inhomogeneity [45]. The Temkin model bases on the assumption of interaction between adsorbent and adsorbate, it defines a linear decreasing relationship between the heat of adsorption  $B$  ( $B = RT/b$ ) and the amount of adsorption. It also describes the chemisorption process as electrostatic interaction [46]. The Sips model accounts for interactions between adsorbed molecules and adsorbent, the model can be simplified to the Freundlich model at lower concentrations, while when  $b_s = 1$ , it can be simplified to the Langmuir model [47].

According to the fitting parameters in Table 5, the isotherms exhibited higher  $R^2$  values for the Freundlich model ( $R^2 = 0.995\text{--}0.997$ ) compared to the Langmuir model ( $R^2 = 0.792\text{--}0.845$ ), indicating that the adsorption process was not a strictly monolayer adsorption, and the inhomogeneous of adsorbent surface led to the possibility of multilayer coverage of adsorbent molecules. The value of  $1/n < 1$  for MAC-750 suggested was favorable for MB adsorption;  $b_s$  in the Sips model (0.0322–0.140) similarly indicated that the adsorbent surface was inhomogeneous, which was consistent with the fitting result of Freundlich

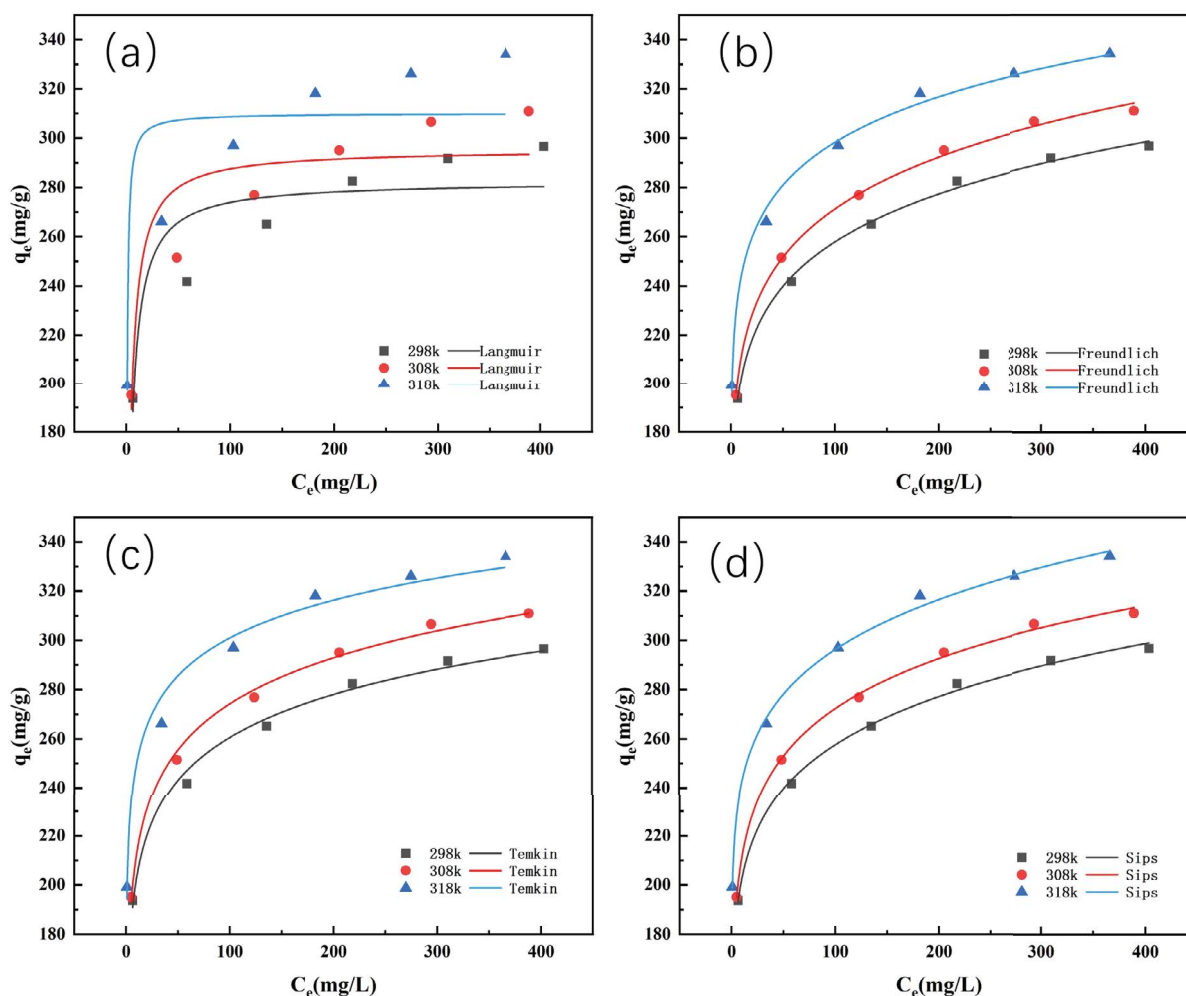


Fig. 8. (a) Langmuir model, (b) Freundlich model, (c) Temkin model, and (d) Sips model of methylene blue adsorption onto MAC-750 at different temperature.

Table 5  
Fitting parameters of the adsorption isotherms of methylene blue adsorption onto MAC-750

Models	Parameters	298 K	308 K	318 K
Langmuir	$q_m$ (mg/g)	283	295	310
	$K_L$ (L/mg)	0.317	0.362	2.16
	$R^2$	0.832	0.845	0.792
Freundlich	$K_f$ (mg/g)	159	165	200
	$n$	9.54	9.26	11.5
	$R^2$	0.997	0.998	0.995
Temkin	$\alpha$ (L/g)	311	263	121
	$\beta$ (J/mol)	94.0	98.0	120
	$B$	26.4	26.1	22.1
Sips	$R^2$	0.992	0.996	0.983
	$K_s$ (L/g)	145	189	89.3
	$a_s$ (L/mg)	0.331	0.171	0.446
Sips	$b_s$	0.0901	0.140	0.0322
	$R^2$	0.997	0.998	0.997

Table 6  
Adsorption capacities of methylene blue onto sludge, straw, steel slag and MAC-750

Adsorbents	Surface area (m <sup>2</sup> /g)	Adsorption capacity of methylene blue (mg/g)
Sludge	8.79	18.8
Straw	1.14	7.36
Steel slag	10.5	14.1
MAC-750	359	283

model. Additionally, the isotherms also fitted well to the Temkin model ( $R^2 = 0.983-0.996$ ), indicating that electrostatic interaction was an important mechanism.

Table 6 presents a comparison of the surface area and methylene blue adsorption capacity of each of the three raw materials with MAC-750. As indicated by the BET results, none of the three raw materials were able to remove methylene blue up to 20 mg/g, suggesting that the activation and pyrolysis processes significantly improved

adsorption capacities. And Table 7 presents a comparison of MB adsorption using various solid-waste-based adsorbents. A literature review revealed that the ACs prepared from different types of sludge or agricultural precursors exhibited a wide scope of methylene blue adsorption capacities, ranging from 13.2 to 323 mg/g. As shown in the table, the investigated MAC demonstrated comparable performance to those reported in the literature.

### 3.6. Studies of adsorption thermodynamic

Adsorption of MB onto MAC-750 has carried out different temperatures for thermodynamic analysis, and the Van't Hoff plots are shown in Fig. 9; the adsorption thermodynamic parameters are presented in Table 8.

Generally, the positive value of  $\Delta H$  lead to an endothermic process, and when the  $\Delta H$  is less than 25 kJ/mol, the adsorption can be attributed to mainly physisorption [53]. In this study, the calculated  $\Delta H$  came to 25.1, 12.2, 14.9 kJ/mol, which suggested the complex progress of the adsorption. The positive value of  $\Delta S$  indicated increased randomness during the adsorption. The negative  $\Delta G$  indicated the MB adsorption onto MAC was thermodynamically favorable and spontaneous at different temperatures [54].

### 3.7. Adsorption mechanism

Through the adsorption studies, the main interactions between MAC and MB include the following:

The trend of methylene blue removal efficiency at different pH values suggests strong electrostatic attraction between the positively charged MB and the negatively charged adsorbent surface. At lower pH conditions, the adsorbent still has a high removal efficiency of MB despite the electrostatic repulsion. And the common salts did not

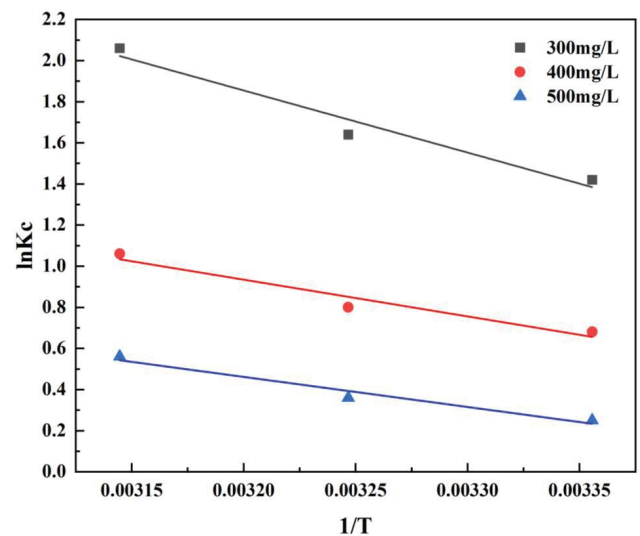


Fig. 9. Effect of temperature on the adsorption of different initial methylene blue concentration.

Table 8

Thermodynamic parameters for the adsorption of different initial methylene blue concentration on MAC-750 at 298, 308 and 318 K

$C_0$ (mg/L)	$\Delta H$ (kJ/mol)	$\Delta S$ (J/(mol·K))	$\Delta G$ (kJ/mol)		
			298 K	308 K	318 K
300	25.1	95.8	-3.58	-4.20	-5.45
400	14.9	55.3	-1.53	-2.05	-2.80
500	12.2	42.8	-0.619	-0.921	-1.480

Table 7

Adsorption of methylene blue onto various solid waste-based adsorbents

Carbon source	Treatment	BET surface area (m <sup>2</sup> /g)	Adsorption capacities for methylene blue (mg/g)	References
Textile sludge	Impregnation With ZnCl <sub>2</sub> and KCl; then pyrolysis at 650°C	221	13.2	[48]
Sewage sludge and corn cob	Carbonized at 550°C, then impregnation with KOH solution, and pyrolysis at 800°C	591	188	[49]
Sewage sludge	Impregnation with ZnCl <sub>2</sub> , pyrolysis at 800°C	765	92.2	[50]
Black liquor lignin and Fenton sludge	Impregnation with KOH, pyrolysis at 800°C	671	184	[51]
Waste orange and lemon peels	Impregnation with 85% H <sub>3</sub> PO <sub>4</sub> , pyrolysis at 600°C for 3 h	168	33.0	[35]
Aerobic granular sludge from a lab-scale SBR	Impregnation with 5 M ZnCl <sub>2</sub> , pyrolysis at 650°C for 2 h	905	323	[52]
Activated sludge	Impregnation with 5 M ZnCl <sub>2</sub> , pyrolysis at 650°C for 2 h	281	144	[52]
Sludge, straw and steel slag	Impregnation with 3 M KOH, pyrolysis with 750°C for 2 h	359	283	This work

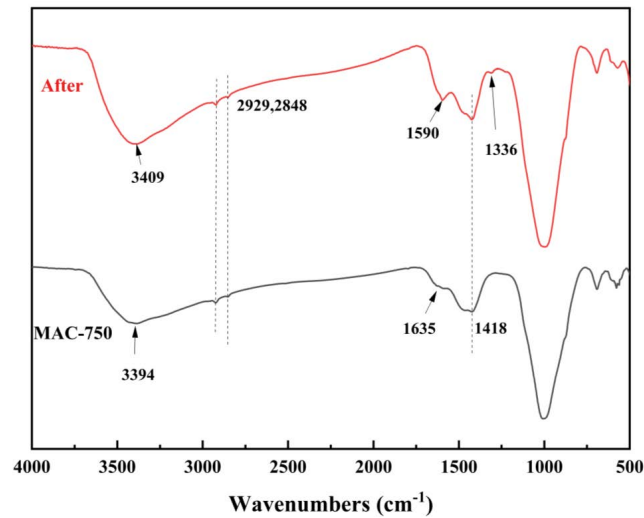


Fig. 10. Fourier-transform infrared spectra of MAC-750 before and after adsorption of methylene blue.

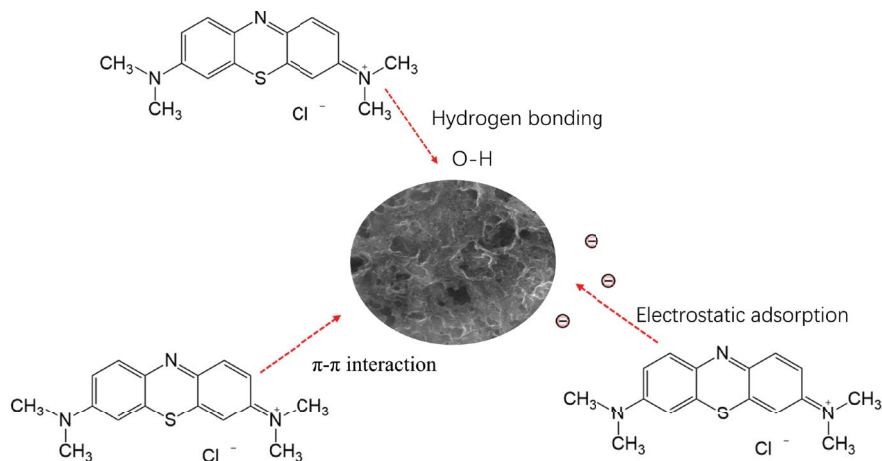


Fig. 11. Image of the adsorption mechanisms.

have a significant effect on the adsorption capacity of methylene blue, indicating that the adsorption process was not controlled by a single factor of electrostatic effect. Fitting results of the kinetic models, isothermal models and studies of adsorption thermodynamics suggest that non-uniform diffusion process and multilayer physisorption were the main process in adsorption, with chemisorption having a relative effect. Fig. 10 shows the FTIR spectra of MAC-750 before and after adsorption, compared with the fresh adsorbent before adsorption, some peaks and their positions changed: a new peak at  $1,336\text{ cm}^{-1}$  was attributed to the  $\text{N-CH}_3$  of the MB [55]; besides, the  $\text{O-H}$  peak at  $3,394$  and  $1,635\text{ cm}^{-1}$  narrowed and shifted, suggested the Nitrogen in methylene blue and  $\text{O-H}$  on the adsorbent surface formed hydrogen bonds and affected the adsorption process [56], the  $\text{C=C}$  peak at  $1,418\text{ cm}^{-1}$  increased, indicated that the  $\pi$ - $\pi$  bond in MB aromatic ring interacted with the  $\pi$ -electron system on the adsorbent surface [57].

The adsorption of methylene blue onto MAC was a complex process and interacted with multiple mechanisms.

On the one hand, the large specific surface area of MACs provided plenty of adsorption sites, which was conducive to the diffusion and migration of MB in the porous structure; on the other hand, the interaction between the adsorbent and the adsorbent provided considerable assistance in the adsorption process. Based on the studies above, the adsorption mechanism was mapped as shown in Fig. 11.

#### 4. Conclusion

The *in-situ* MAC was prepared successfully by synergistically utilizing the characteristics of multiple solid wastes. It demonstrated excellent adsorption capacity of MB. Besides, the magnetic properties provided by the reduced  $\text{Fe}_3\text{O}_4$  and  $\text{Fe}^0$  facilitated the separation of the adsorbent from wastewater, providing an additional advantage. Batch adsorption experiments suggested that MAC had good removal efficiency under different adsorption conditions. Kinetics, isotherm and thermodynamics studies showed that the adsorption process involved both physisorption

and chemisorption on an inhomogeneous surface and was spontaneous and endothermic. The adsorption mechanisms were dominated by the electrostatic attraction,  $\pi$ -electron system interaction and hydrogen bond formation.

In conclusion, the MAC prepared is environmentally friendly, inexpensive, easy to produce, with high adsorption efficiency and significant magnetic separation effect, which provides a new way in the green reuse of multiple solid waste.

### Acknowledgement

This work was financially supported by National Key Research and Development Project of China (2019YFC1904601).

### Declaration of competing interest

The authors declare that they have no known competing financial interests or personal relationships that could have appeared to influence the work reported in this paper.

### Data availability statement

All relevant data are included in the paper or its Supplementary Information.

### References

- [1] M.M. Iqbal, M. Imran, T. Hussain, M.A. Naeem, A.A. Al-Kahtani, G.M. Shah, S. Ahmad, A. Farooq, M. Rizwan, A. Majeed, A.R. Khan, S. Ali, Effective sequestration of Congo red dye with ZnO/cotton stalks biochar nanocomposite: MODELING, reusability and stability, *J. Saudi Chem. Soc.*, 25 (2021) 101176, doi: 10.1016/j.jscs.2020.101176.
- [2] G. Zhao, C. Li, X. Wu, J. Yu, X. Jiang, W. Hu, F. Jiao, Reduced graphene oxide modified NiFe-calcinated layered double hydroxides for enhanced photocatalytic removal of methylene blue, *Appl. Surf. Sci.*, 434 (2018) 251–259.
- [3] M. Rafatullah, O. Sulaiman, R. Hashim, A. Ahmad, Adsorption of methylene blue on low-cost adsorbents: a review, *J. Hazard. Mater.*, 177 (2010) 70–80.
- [4] L. Ren, G. Zhao, L. Pan, B. Chen, Y. Chen, Q. Zhang, X. Xiao, W. Xu, Efficient removal of dye from wastewater without selectivity using activated carbon-juncus effusus porous fibril composites, *ACS Appl. Mater. Interfaces*, 13 (2021) 19176–19186.
- [5] N. Gao, K. Kamran, C. Quan, P.T. Williams, Thermochemical conversion of sewage sludge: a critical review, *Prog. Energy Combust. Sci.*, 79 (2020) 100843, doi: 10.1016/j.pecs.2020.100843.
- [6] L. Dhote, S. Kumar, L. Singh, R. Kumar, A systematic review on options for sustainable treatment and resource recovery of distillery sludge, *Chemosphere*, 263 (2021) 128225, doi: 10.1016/j.chemosphere.2020.128225.
- [7] S.S.A. Syed-Hassan, Y. Wang, S. Hu, S. Su, J. Xiang, Thermochemical processing of sewage sludge to energy and fuel: fundamentals, challenges and considerations, *Renewable Sustainable Energy Rev.*, 80 (2017) 888–913.
- [8] L.P. Wang, Y.Z. Chang, A.M. Li, Hydrothermal carbonization for energy-efficient processing of sewage sludge: a review, *Renewable Sustainable Energy Rev.*, 108 (2019) 423–440.
- [9] L.J. Leng, X.Z. Yuan, H.J. Huang, J.G. Shao, H. Wang, X.H. Chen, G.M. Zeng, Biochar derived from sewage sludge by liquefaction: characterization and application for dye adsorption, *Appl. Surf. Sci.*, 346 (2015) 223–231.
- [10] W.W. Li, Z.L. Han, D.Z. Sun, Preparation of sludge-based activated carbon for adsorption of dimethyl sulfide and dimethyl disulfide during sludge aerobic composting, *Chemosphere*, 279 (2021) 130924, doi: 10.1016/j.chemosphere.2021.130924.
- [11] N.M.Y. Almahbashi, S.R.M. Kutty, M. Ayoub, A. Noor, I.U. Salihi, A. Al-Nini, A.H. Jagaba, B.N.S. Aldhawi, A.A.S. Ghaleb, Optimization of preparation conditions of sewage sludge based activated carbon, *Ain Shams Eng. J.*, 12 (2021) 1175–1182.
- [12] Q. Liang, Y. Liu, M. Chen, L. Ma, B. Yang, L. Li, Q. Liu, Optimized preparation of activated carbon from coconut shell and municipal sludge, *Mater. Chem. Phys.*, 241 (2020) 122327, doi: 10.1016/j.matchemphys.2019.122327.
- [13] B. Yang, Y. Liu, Q. Liang, M. Chen, L. Ma, L. Li, Q. Liu, W. Tu, D. Lan, Y. Chen, Evaluation of activated carbon synthesized by one-stage and two-stage co-pyrolysis from sludge and coconut shell, *Ecotoxicol. Environ. Saf.*, 170 (2019) 722–731.
- [14] X. Kang, Y. Liu, C. Yang, H. Cheng, Removal of amoxicillin from aqueous solution using sludge-based activated carbon modified by walnut shell and nano-titanium dioxide, *Water Reuse*, 11 (2021) 97–109.
- [15] L.Z. Lee, M.A.A. Zaini, One-step ZnCl<sub>2</sub>/FeCl<sub>3</sub> composites preparation of magnetic activated carbon for effective adsorption of Rhodamine B dye, *Toxin Rev.*, 41 (2022) 64–81.
- [16] Z.H. Xu, Y.W. Zhou, Z.H. Sun, D.F. Zhang, Y.X. Huang, S.Y. Gu, W.F. Chen, Understanding reactions and pore-forming mechanisms between waste cotton woven and FeCl<sub>3</sub> during the synthesis of magnetic activated carbon, *Chemosphere*, 241 (2020) 125120, doi: 10.1016/j.chemosphere.2019.125120.
- [17] G.Z. Kyzas, E.A. Deliyanni, N.K. Lazaridis, Magnetic modification of microporous carbon for dye adsorption, *J. Colloid Interface Sci.*, 430 (2014) 166–173.
- [18] H.B. Wang, J.Y. Cai, Z.W. Liao, A. Jawad, J. Iftthikar, Z.L. Chen, Z.Q. Chen, Black liquor as biomass feedstock to prepare zero-valent iron embedded biochar with red mud for Cr(VI) removal: mechanisms insights and engineering practicality, *Bioresour. Technol.*, 311 (2020) 123553, doi: 10.1016/j.biortech.2020.123553.
- [19] O. Kazak, Fabrication of *in-situ* magnetic activated carbon by co-pyrolysis of sucrose with waste red mud for removal of Cr(VI) from waters, *Environ. Technol. Innovation*, 24 (2021) 101856, doi: 10.1016/j.eti.2021.101856.
- [20] H. Yi, G.P. Xu, H.G. Cheng, J.S. Wang, Y.F. Wan, H. Chen, An Overview of Utilization of Steel Slag, *Proceedings of the 7th International Conference on Waste Management and Technology (ICWMT)*, Beijing, China, 5–7 September 2012, pp. 791–801.
- [21] S. Wu, Y. Xue, Q. Ye, Y. Chen, Utilization of steel slag as aggregates for stone mastic asphalt (SMA) mixtures, *Build. Environ.*, 42 (2007) 2580–2585.
- [22] L.V. Thuan, T.B. Chau, T.T.K. Ngan, T.X. Vu, D.D. Nguyen, M.H. Nguyen, D.T.T. Thao, N.T. Hoai, L.H. Sinh, Preparation of cross-linked magnetic chitosan particles from steel slag and shrimp shells for removal of heavy metals, *Environ. Technol.*, 39 (2018) 1745–1752.
- [23] A.A. Basaleh, M.H. Al-Malack, T.A. Saleh, Poly(acrylamide acrylic acid) grafted on steel slag as an efficient magnetic adsorbent for cationic and anionic dyes, *J. Environ. Chem. Eng.*, 9 (2021) 105126, doi: 10.1016/j.jece.2021.105126.
- [24] M. Thommes, K. Kaneko, A.V. Neimark, J.P. Olivier, F. Rodriguez-Reinoso, J. Rouquerol, K.S.W. Sing, Physisorption of gases, with special reference to the evaluation of surface area and pore size distribution (IUPAC Technical Report), *Pure Appl. Chem.*, 87 (2015) 1051–1069.
- [25] X. Li, Y. Wei, J. Xu, N. Xu, Y. He, Quantitative visualization of lignocellulose components in transverse sections of moso bamboo based on FTIR macro- and micro-spectroscopy coupled with chemometrics, *Biotechnol. Biofuels*, 11 (2018) 263, doi: 10.1186/s13068-018-1251-4.
- [26] M.S. Netto, N.F. da Silva, E.S. Mallmann, G.L. Dotto, E.L. Foletto, Effect of salinity on the adsorption behavior of methylene blue onto comminuted raw avocado residue: CCD-RSM design, *Water Air Soil Pollut.*, 230 (2019) 187, doi: 10.1007/s11270-019-4230-x.
- [27] B. Yang, Y.C. Liu, Q.L. Liang, M.Y. Chen, L.L. Ma, L.L. Li, Q. Liu, W.W. Tu, D.W. Lan, Y.Y. Chen, Evaluation of activated carbon synthesized by one-stage and two-stage co-pyrolysis from sludge and coconut shell, *Ecotoxicol. Environ. Saf.*, 170 (2019) 722–731.

- [28] S.H. Tang, M.A.A. Zaini, Malachite green adsorption by potassium salts-activated carbons derived from textile sludge: equilibrium, kinetics and thermodynamics studies, *Asia-Pac. J. Chem. Eng.*, 12 (2017) 159–172.
- [29] B. Li, Y. Zhang, J. Xu, S.S. Fan, H.C. Xu, Facile preparation of magnetic porous biochars from tea waste for the removal of tetracycline from aqueous solutions: effect of pyrolysis temperature, *Chemosphere*, 291 (2022) 132713, doi: 10.1016/j.chemosphere.2021.132713.
- [30] E. Koseoglu, C. Akmil-Basar, Preparation, structural evaluation and adsorptive properties of activated carbon from agricultural waste biomass, *Adv. Powder Technol.*, 26 (2015) 811–818.
- [31] K.D. Gong, Q. Hu, L. Yao, M. Li, D.Z. Sun, Q. Shao, B. Qiu, Z.H. Guo, Ultrasonic pretreated sludge derived stable magnetic active carbon for Cr(VI) removal from wastewater, *ACS Sustainable Chem. Eng.*, 6 (2018) 7283–7291.
- [32] D.W. Cho, K. Yoon, Y. Ahn, Y.Q. Su, D.C.W. Tsang, D.Y. Hou, Y.S. Ok, H. Son, Fabrication and environmental applications of multifunctional mixed metal-biochar composites (MMBC) from red mud and lignin wastes, *J. Hazard. Mater.*, 374 (2019) 412–419.
- [33] S. Jodeh, O. Hamed, A. Melhem, R. Salghi, D. Jodeh, K. Azzaoui, Y. Benmassaoud, K. Murtada, Magnetic nanocellulose from olive industry solid waste for the effective removal of methylene blue from wastewater, *Environ. Sci. Pollut. Res.*, 25 (2018) 22060–22074.
- [34] A.A. Inyinbor, F.A. Adekola, G.A. Olatunji, Kinetics, isotherms and thermodynamic modeling of liquid phase adsorption of Rhodamine B dye onto *Raphia hookerie* fruit epicarp, *Water Resour. Ind.*, 15 (2016) 14–27.
- [35] D. Ramutshatsha-Makhwedzha, A. Mavhungu, M.L. Moropeng, R. Mbaya, Activated carbon derived from waste orange and lemon peels for the adsorption of methyl orange and methylene blue dyes from wastewater, *Heliyon*, 8 (2022) e09930, doi: 10.1016/j.heliyon.2022.e09930.
- [36] X.J. Liu, M.F. Li, S.K. Singh, Manganese-modified lignin biochar as adsorbent for removal of methylene blue, *J. Mater. Res. Technol.*, 12 (2021) 1434–1445.
- [37] S. Afroze, T.K. Sen, M. Ang, H. Nishioka, Adsorption of methylene blue dye from aqueous solution by novel biomass *Eucalyptus sheathiana* bark: equilibrium, kinetics, thermodynamics and mechanism, *Desal. Water Treat.*, 57 (2016) 5858–5878.
- [38] M. Fedoseeva, P. Fita, A. Punzi, E. Vauthey, Salt effect on the formation of dye aggregates at liquid/liquid interfaces studied by time-resolved surface second harmonic generation, *J. Phys. Chem. C*, 114 (2010) 13774–13781.
- [39] W. Huang, M. Zhang, Y.H. Wang, J. Chen, J.Q. Zhang, Biochars prepared from rabbit manure for the adsorption of Rhodamine B and Congo red: characterisation, kinetics, isotherms and thermodynamic studies, *Water Sci. Technol.*, 81 (2020) 436–444.
- [40] T. Maneerung, J. Liew, Y.J. Dai, S. Kawi, C. Chong, C.H. Wang, Activated carbon derived from carbon residue from biomass gasification and its application for dye adsorption: kinetics, isotherms and thermodynamic studies, *Bioresour. Technol.*, 200 (2016) 350–359.
- [41] Z.L. Zhang, Y. Li, L. Ding, J. Yu, Q. Zhou, Y.L. Kong, J.Y. Ma, Novel sodium bicarbonate activation of cassava ethanol sludge derived biochar for removing tetracycline from aqueous solution: performance assessment and mechanism insight, *Bioresour. Technol.*, 330 (2021) 124949, doi: 10.1016/j.biortech.2021.124949.
- [42] F.Q. Guo, X.L. Li, X.C. Jiang, X.M. Zhao, C.L. Guo, Z.H. Rao, Characteristics and toxic dye adsorption of magnetic activated carbon prepared from biomass waste by modified one-step synthesis, *Colloids Surf., A*, 555 (2018) 43–54.
- [43] E. Malkoc, Y. Nuhoglu, Potential of tea factory waste for chromium(VI) removal from aqueous solutions: thermodynamic and kinetic studies, *Sep. Purif. Technol.*, 54 (2007) 291–298.
- [44] K. Kadirvelu, C. Namasivayam, Activated carbon from coconut coirpith as metal adsorbent: adsorption of Cd(II) from aqueous solution, *Adv. Environ. Res.*, 7 (2003) 471–478.
- [45] C. Jung, J. Heo, J. Han, N. Her, S.J. Lee, J. Oh, J. Ryu, Y. Yoon, Hexavalent chromium removal by various adsorbents: powdered activated carbon, chitosan, and single/multi-walled carbon nanotubes, *Sep. Purif. Technol.*, 106 (2013) 63–71.
- [46] D. Kavitha, C. Namasivayam, Experimental and kinetic studies on methylene blue adsorption by coir pith carbon, *Bioresour. Technol.*, 98 (2007) 14–21.
- [47] K. Vijayaraghavan, T.V.N. Padmesh, K. Palanivelu, M. Velan, Biosorption of nickel(II) ions onto *Sargassum wightii*: application of two-parameter and three-parameter isotherm models, *J. Hazard. Mater.*, 133 (2006) 304–308.
- [48] S. Wong, N.A.N. Yac'cob, N. Ngadi, O. Hassan, I.M. Inuwa, From pollutant to solution of wastewater pollution: synthesis of activated carbon from textile sludge for dye adsorption, *Chin. J. Chem. Eng.*, 26 (2018) 870–878.
- [49] C.Z. Wu, M. Song, B.S. Jin, Y.M. Wu, Y.J. Huang, Effect of biomass addition on the surface and adsorption characterization of carbon-based adsorbents from sewage sludge, *J. Environ. Sci.*, 25 (2013) 405–412.
- [50] Y.H. Li, F.M. Chang, B. Huang, Y.P. Song, H.Y. Zhao, K.J. Wang, Activated carbon preparation from pyrolysis char of sewage sludge and its adsorption performance for organic compounds in sewage, *Fuel*, 266 (2020) 117053, doi: 10.1016/j.fuel.2020.117053.
- [51] R.Y. Zhu, J. Xia, H.J. Zhang, F.G. Kong, X. Hu, Y.A. Shen, W.H. Zhang, Synthesis of magnetic activated carbons from black liquor lignin and Fenton sludge in a one-step pyrolysis for methylene blue adsorption, *J. Environ. Chem. Eng.*, 9 (2021) 106538, doi: 10.1016/j.jece.2021.106538.
- [52] X. Ding, H. Chen, Q. Yang, J. Wei, D. Wei, Effect of sludge property on the synthesis, characterization and sorption performance of sludge-based biochar, *Bioresour. Technol. Rep.*, 7 (2019) 100204, doi: 10.1016/j.biteb.2019.100204.
- [53] S.S. Fan, Y. Wang, Z. Wang, J. Tang, J. Tang, X.D. Li, Removal of methylene blue from aqueous solution by sewage sludge-derived biochar: adsorption kinetics, equilibrium, thermodynamics and mechanism, *J. Environ. Chem. Eng.*, 5 (2017) 601–611.
- [54] L. Borah, M. Goswami, P. Phukan, Adsorption of methylene blue and eosin yellow using porous carbon prepared from tea waste: adsorption equilibrium, kinetics and thermodynamics study, *J. Environ. Chem. Eng.*, 3 (2015) 1018–1028.
- [55] J. Gong, J. Liu, Z.W. Jiang, X. Wen, E. Mijowska, T. Tang, X.C. Chen, A facile approach to prepare porous cup-stacked carbon nanotube with high performance in adsorption of methylene blue, *J. Colloid Interface Sci.*, 445 (2015) 195–204.
- [56] M. Mariana, E.M. Mistar, T. Alfatah, M.D. Supardan, High-porous activated carbon derived from *Myristica fragrans* shell using one-step KOH activation for methylene blue adsorption, *Bioresour. Technol. Rep.*, 16 (2021) 100845, doi: 10.1016/j.biteb.2021.100845.
- [57] A.H. Jawad, A.S. Abdulhameed, Statistical modeling of methylene blue dye adsorption by high surface area mesoporous activated carbon from bamboo chip using KOH-activated thermal activation, *Energy Ecol. Environ.*, 5 (2020) 456–469.